Supplement of Atmos. Chem. Phys., 26, 4823–4840, 2026
https://doi.org/10.5194/acp-26-4823-2026-supplement

Atmospheric Chemistry and Physics
Open Access
EGU

Supplement of

Mechanistic investigations of the formation of multifunctional products from the multi-generation •OH oxidation of styrene

Long Chen et al.

Correspondence to: Yu Huang (huangyu@ieecas.cn)

Table S1 The energy barriers (ΔE_a in kcal/mol) of all the elementary reactions involved in the initial addition of OH radical to styrene and intramolecular H-shift reactions of first generation peroxyl radicals S2-1-x calculated at the DLPNO-CCSD(T)/aug-cc-pVTZ and M06-2X/6-311++G(3df,3pd) levels

Entry	DLPNO-CCSD(T)/aug-cc-pVTZ	M06-2X/6-311++G(3df,3pd)
R_{TS1}	0.4	0.8
$R_{TS2\text{-}1\text{-}a}$	21.5	21.0
$R_{TS2\text{-}1\text{-}b}$	32.4	33.3
$R_{TS2\text{-}1\text{-}c}$	32.6	33.6
$R_{TS2\text{-}1\text{-}d}$	27.5	27.9
$R_{TS2\text{-}1\text{-}e}$	30.1	31.3
$R_{TS2\text{-}1\text{-}f}$	31.0	31.1
$R_{TS2\text{-}1\text{-}h}$	30.5	30.6
$R_{TS3\text{-}1\text{-}a}$	1.3	0.8

Table S2 The relative electronic energy (ΔE_i), free energy (ΔG_i) and Boltzmann population (w_i) of different conformers involved in the first generation peroxy radicals S2-1-x predicted at the M06-2X/6-311++G(3df,3pd)//M06-2X/6-31+G(d,p) level

Conformer	ΔE_i(kcal/mol)	ΔG_i(kcal/mol)	w_i
S2-1-a	0.00	0.00	57.32%
S2-1-b	0.18	0.36	31.21%
S2-1-c	1.34	1.08	9.25%
S2-1-d	2.58	2.51	0.83%
S2-1-e	2.87	2.88	0.44%
S2-1-f	2.98	3.18	0.27%
S2-1-g	3.58	2.86	0.46%
S2-1-h	3.60	3.27	0.23%

Table S3 The energy barriers (ΔE_a in kcal/mol) of the addition OH radical to the different sites of 1st-ROOH (S4) calculated at the DLPNO-CCSD(T)/aug-cc-pVTZ//M06-2X/6-311+G(d,p) and M06-2X/6-311++G(3df,3pd)//M06-2X/6-31+g(d,p)levels

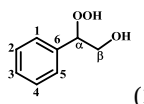 (1st-ROOH (S4))	DLPNO-CCSD(T)/aug-cc-pVTZ// M06-2X/6-311+G(d,p)	M06-2X/6-311++G(3df,3pd)// M06-2X/6-31+g(d,p)
syn-OH-addition (OH is added in the same direction of -OOH group)		
C1-site	3.3	3.6

C2-site	7.8	8.8
C3-site	8.4	9.5
C4-site	5.4	5.7
C5-site	5.0	6.2
C6-site	4.7	5.8
anti-OH-addition (OH is added in the opposite direction of -OOH group)		
C1-site	2.0	0.8
C2-site	6.3	5.3
C3-site	6.7	6.0
C4-site	5.7	4.7
C5-site	2.6	1.4
C6-site	5.2	4.3

Table S4 The relative electronic energy (ΔE_i), free energy (ΔG_i) and Boltzmann population (w_i) of different conformers involved in S8-x predicted at the M06-2X/6-311++G(3df,3pd)//M06-2X/6-31+G(d,p) level

Conformer	ΔE_i(kcal/mol)	ΔG_i(kcal/mol)	w_i
S8-a	0.00	0.00	85.78%
S8-b	1.27	1.20	11.30%
S8-c	1.75	2.43	1.42%
S8-d	2.44	2.58	1.10%
S8-e	2.86	3.18	0.40%

Table S5 The energy barrier (ΔE_a), IRC-TST rate coefficient ($k_{IRC\text{-}TST}$), Boltzmann populations (w_i) of conformer *i*, and MC-TST rate coefficient ($k_{MC\text{-}TST}$) involved in S8-x calculated at the M06-2X/6-311++G(3df,3pd)//M06-2X/6-31+G(d,p) level

Reactions	ΔE_a(kcal/mol)	$k_{IRC\text{-}TST}$ (s^{-1})	w_i	$k_{MC\text{-}TST}$(s^{-1})
S8-a → S8-a-P	24.3	4.3×10^{-4}	85.78%	8.2×10^{9}
S8-b → S8-b-P	8.4	3.1×10^{6}	11.30%	
S8-c → S8-c-P	0.6	5.8×10^{11}	1.42%	
S8-d → S8-d-P	34.2	7.2×10^{-10}	1.10%	
S8-e → S8-e-P	11.8	5.4×10^{4}	0.40%	

Table S6 The relative electronic energy (ΔE_i), free energy (ΔG_i) and Boltzmann population (w_i) of different conformers involved in S28-x predicted at the M06-2X/6-311++G(3df,3pd)//M06-2X/6-31+G(d,p) level

Conformer	ΔE_i(kcal/mol)	ΔG_i(kcal/mol)	w_i
S28-a	0.00	0.00	88.79%
S28-b	1.50	1.41	8.21%
S28-c	1.97	2.11	2.52%
S28-d	3.88	3.14	0.44%
S28-e	4.49	4.42	0.05%

Table S7 The activation energy (ΔE_a), IRC-TST rate coefficient ($k_{IRC\text{-}TST}$), Boltzmann populations (w_i) of conformer *i*, and MC-TST rate coefficient ($k_{MC\text{-}TST}$) involved in S28-x calculated at the M06-2X/6-311++G(3df,3pd)//M06-2X/6-31+G(d,p) level

Reactions	ΔE_a(kcal/mol)	$k_{IRC\text{-}TST}$ (s^{-1})	w_i	$k_{MC\text{-}TST}$(s^{-1})
S28-a → S28-a-P	12.7	8.9×10^{4}	88.79%	1.7×10^{9}
S28-b → S28-b-P	25.6	6.2×10^{-4}	8.21%	
S28-c → S28-c-P	38.3	7.3×10^{-12}	2.52%	
S28-d → S28-d-P	6.0	5.1×10^{7}	0.44%	
S28-e → S28-e-P	2.0	3.4×10^{10}	0.05%	

Table S8 Predicted saturated vapour pressure (P^0) and saturated concentrations (c^0) of styrene and its multi-generation OH oxidation closed-shell products

	Species	P^0 (atm)	c^0 (ug/m^3)	Species	P^0 (atm)	c^0 (ug/m^3)
Initial reactant	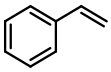 Styrene (C_8H_8) VOC	4.63×10^{-3}	1.95×10^{7}			
First generation products	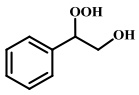 S4 ($C_8H_{10}O_3$) IVOC	1.43×10^{-7}	8.89×10^{2}	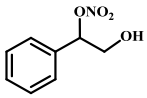 S5 ($C_8H_9NO_3$) IVOC	2.54×10^{-7}	1.87×10^{3}
	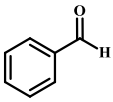 Benzaldehyde (C_7H_6O) VOC	7.62×10^{-4}	2.89×10^{6}			
Second generation products	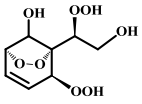 S6 ($C_8H_{12}O_8$) LVOC	4.72×10^{-12}	4.50×10^{-2}	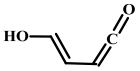 S10 ($C_4H_4O_2$) VOC	6.41×10^{-4}	2.17×10^{6}

	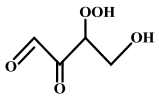 S10-2 ($C_4H_6O_5$) IVOC	1.83×10^{-7}	9.91×10^{2}	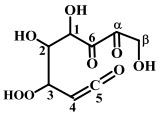 S13 ($C_8H_{10}O_8$) LVOC	5.11×10^{-9}	2.97×10^{-2}
	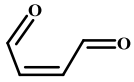 S14 ($C_4H_4O_2$) VOC	2.48×10^{-3}	8.39×10^{6}	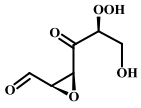 S20 ($C_6H_8O_6$) SVOC	5.11×10^{-9}	42.21
	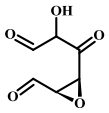 S23 ($C_6H_6O_5$) IVOC	6.73×10^{-8}	4.31×10^{2}			
	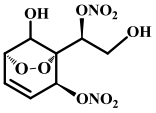 S26 ($C_8H_{10}N_2O_{10}$) LVOC	1.52×10^{-11}	0.18	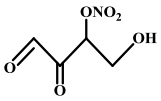 S30-2 ($C_4H_5NO_6$) IVOC	3.29×10^{-7}	2.16×10^{3}
	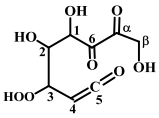 S33 ($C_8H_{10}O_8$) LVOC	5.11×10^{-9}	2.97×10^{-2}	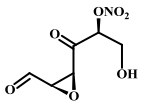 S40-1 ($C_6H_7NO_7$) SVOC	9.16×10^{-9}	75.86
	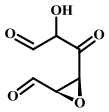 S40-2 ($C_6H_6O_5$) IVOC	6.73×10^{-8}	4.31×10^{2}			
Third generation products	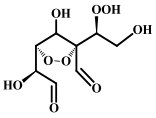 S47 ($C_8H_{12}O_9$) LVOC	2.64×10^{-14}	2.68×10^{-4}	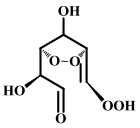 S48 ($C_6H_8O_7$) SVOC	4.63×10^{-10}	3.59
	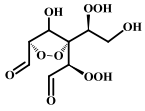 S51($C_8H_{12}O_{10}$) LVOC	1.46×10^{-14}	1.58×10^{-4}	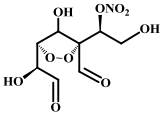 S58 ($C_8H_{11}NO_{10}$) LVOC	4.73×10^{-14}	5.37×10^{-4}

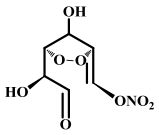	1.14×10^{-9}	10.16	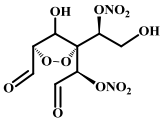	4.70×10^{-14}	6.18×10^{-4}
S59 ($C_6H_7NO_8$)			S62 ($C_8H_{10}N_2O_{12}$)		
SVOC			LVOC		

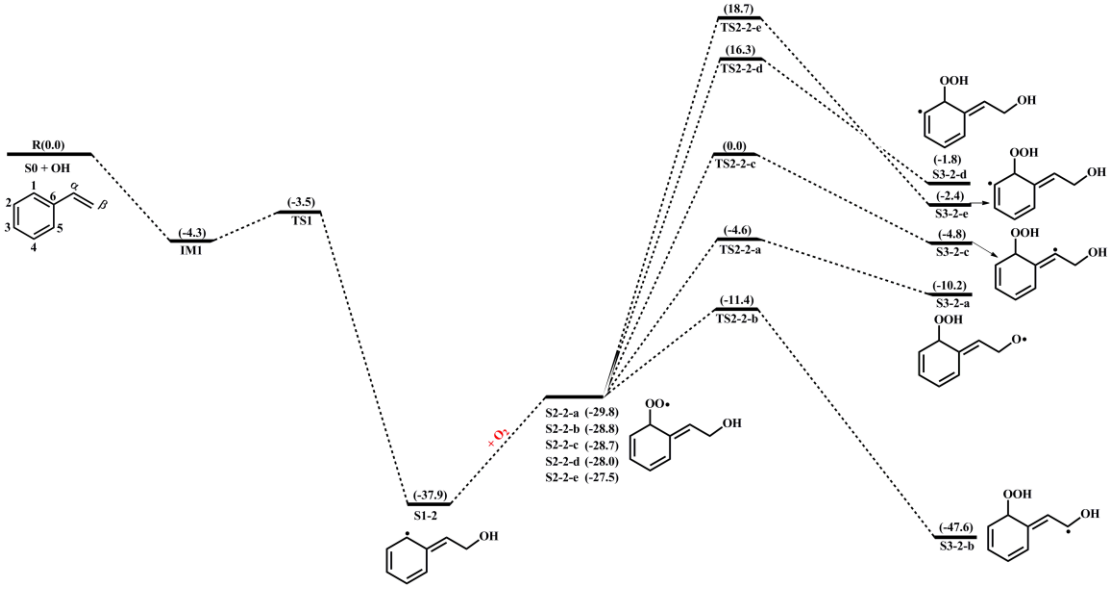

Figure S1. PES for the OH-initiated oxidation of styrene and the unimolecular reactions of S2-2-x at the M06-2X/6-311++G(3df,3pd)//M06-2X/6-31+g(d,p) level

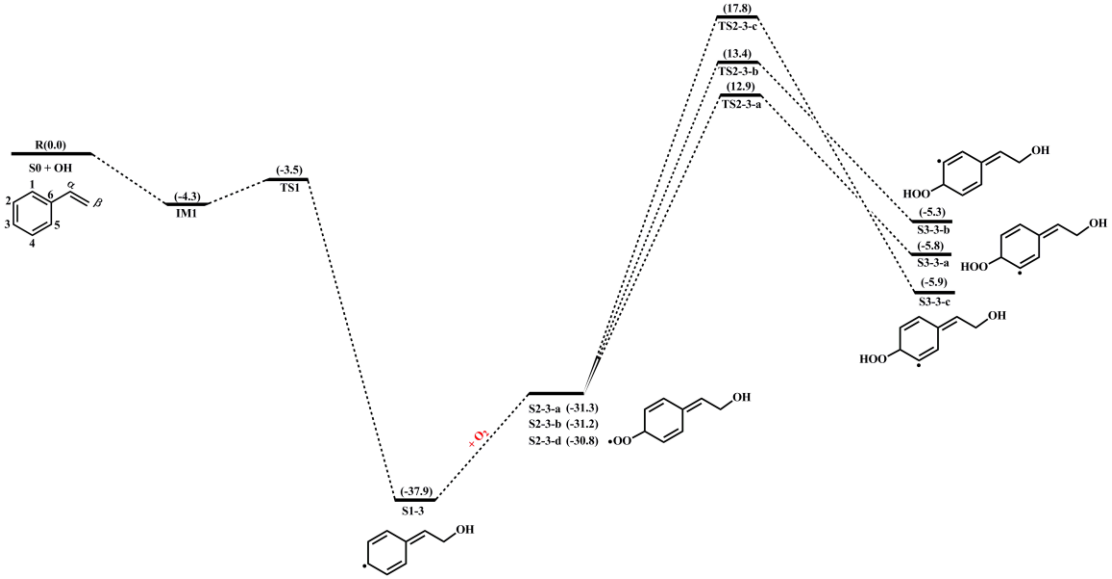

Figure S2. PES for the OH-initiated oxidation of styrene and the unimolecular reactions of S2-3-x at the M06-2X/6-311++G(3df,3pd)//M06-2X/6-31+g(d,p) level

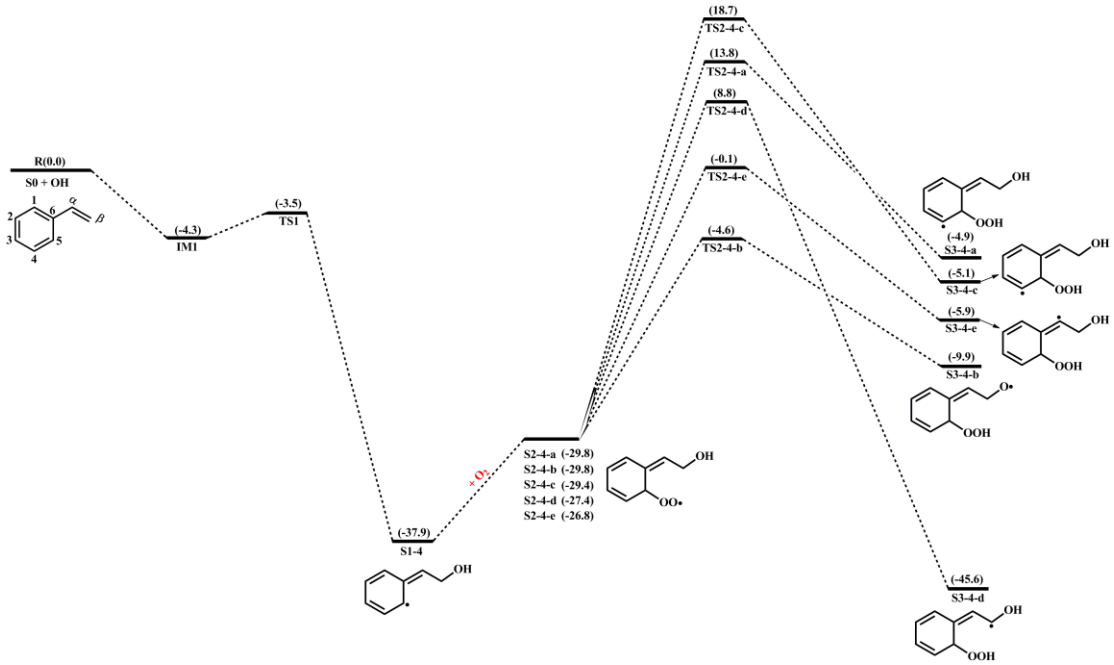

Figure S3. PES for the OH-initiated oxidation of styrene and the unimolecular reactions of S2-4-x at the M06-2X/6-311++G(3df,3pd)//M06-2X/6-31+g(d,p) level

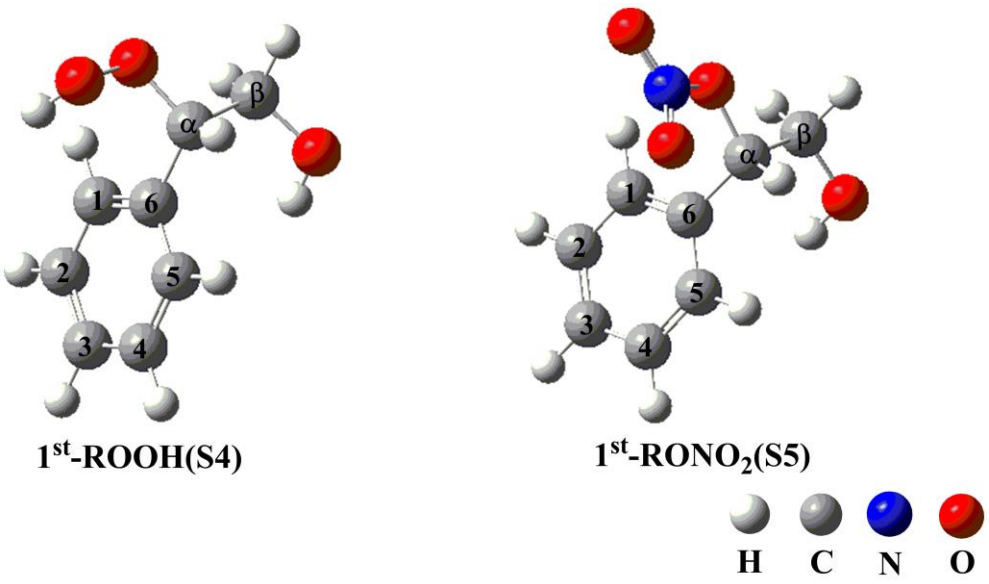

Figure S4. Global minimum structures of 1^{st}-ROOH(S4) and 1^{st}-$RONO_2$(S5) at the M06-2X/6-31+g(d,p) level

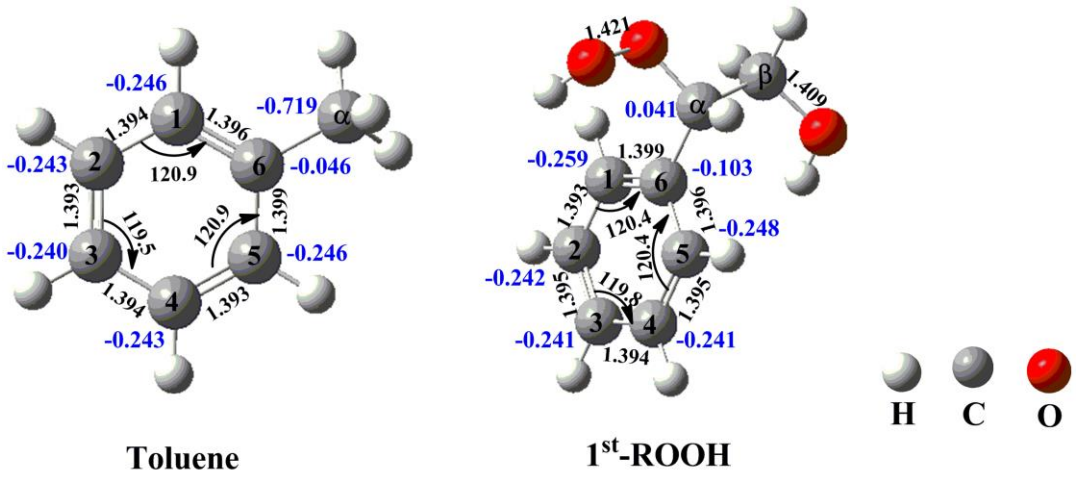

Figure S5. The geometric parameters of toluene and 1[st]-ROOH (S4) and the NPA atomic charges (blue font) of all the carbon atoms in the benzene ring predicted at the M06-2X/6-31+g(d,p) level

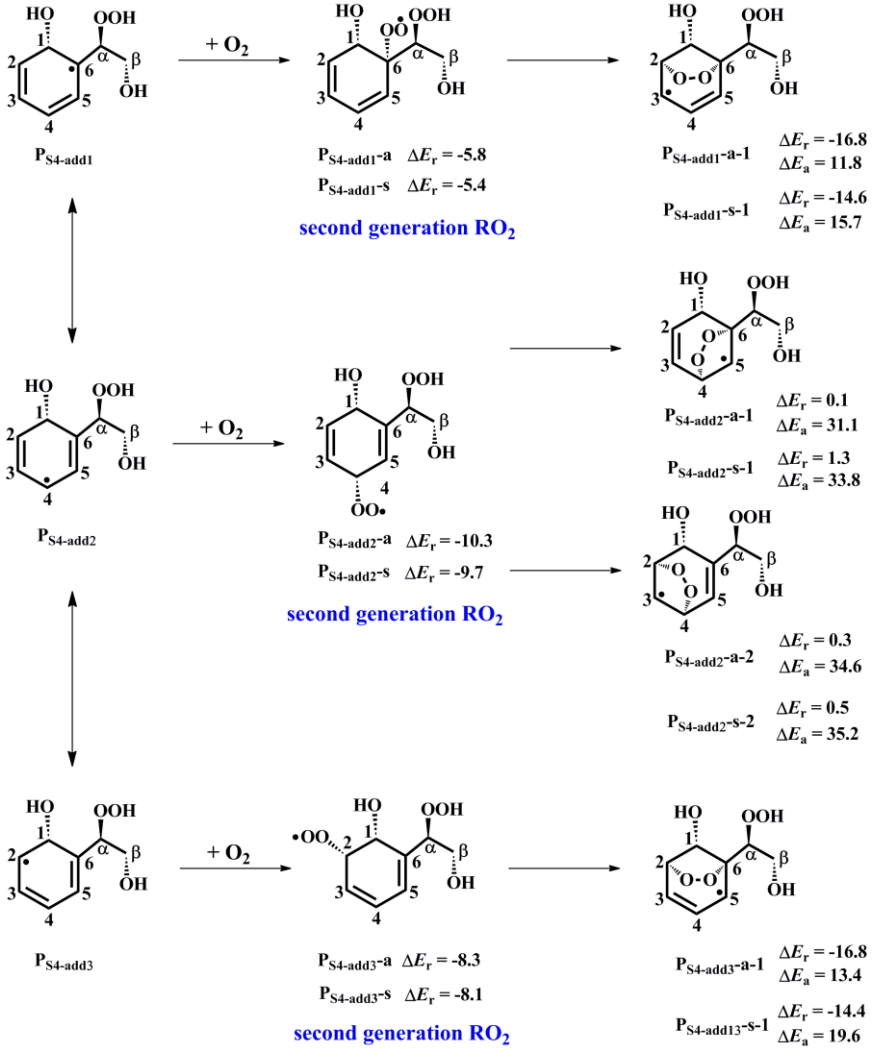

Figure S6. PES for the addition reactions $P_{S4\text{-}add1}$ + O_2 and subsequent intramolecular cyclization reactions at the M06-2X/6-311++G(3df,3pd)//M06-2X/6-31+g(d,p) level (the symbols s and a represent *syn*- and *anti*-O_2-addition)

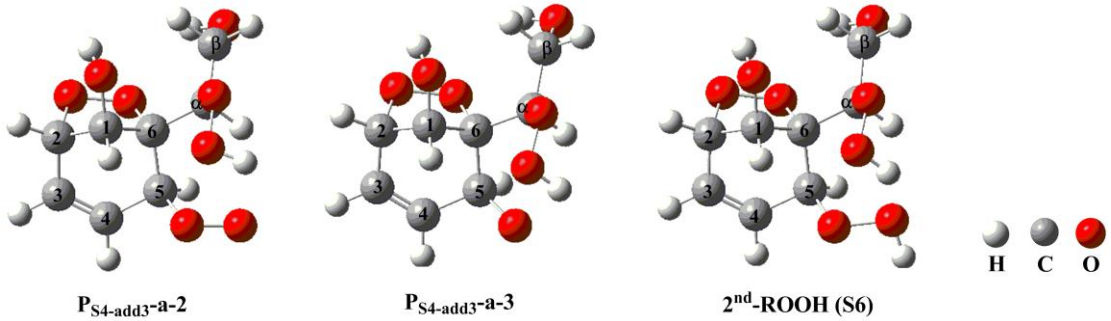

Figure S7. The lowest energy conformers of third generation peroxy radical $P_{S4\text{-}add3}$-a-2, peroxide bicyclic alkoxy radical $P_{S4\text{-}add3}$-a-3 and the second generation product bicyclic hydroperoxide 2^{nd}-ROOH(S6) at the M06-2X/6-31+g(d,p) level

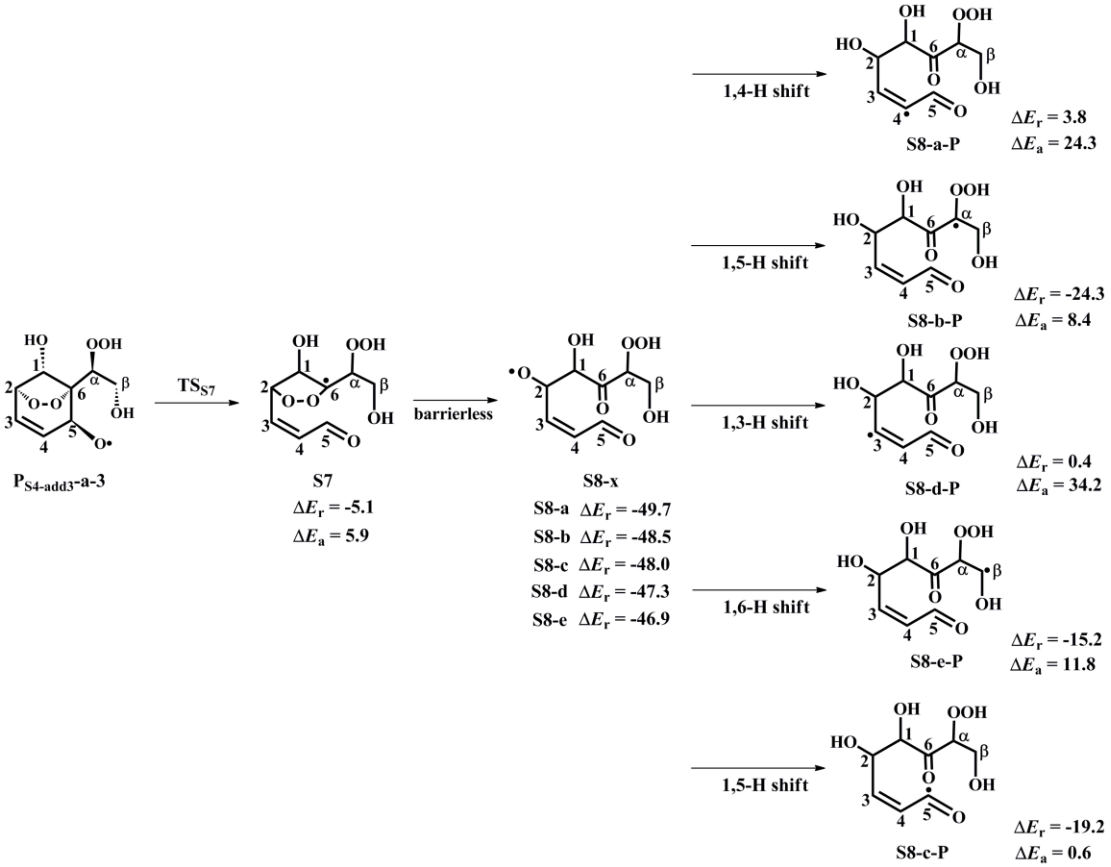

Figure S8. PES for the intramolecular hydrogen transfer reactions of S8-x at the M06-2X/6-311++G(3df,3pd)//M06-2X/6-31+g(d,p) level

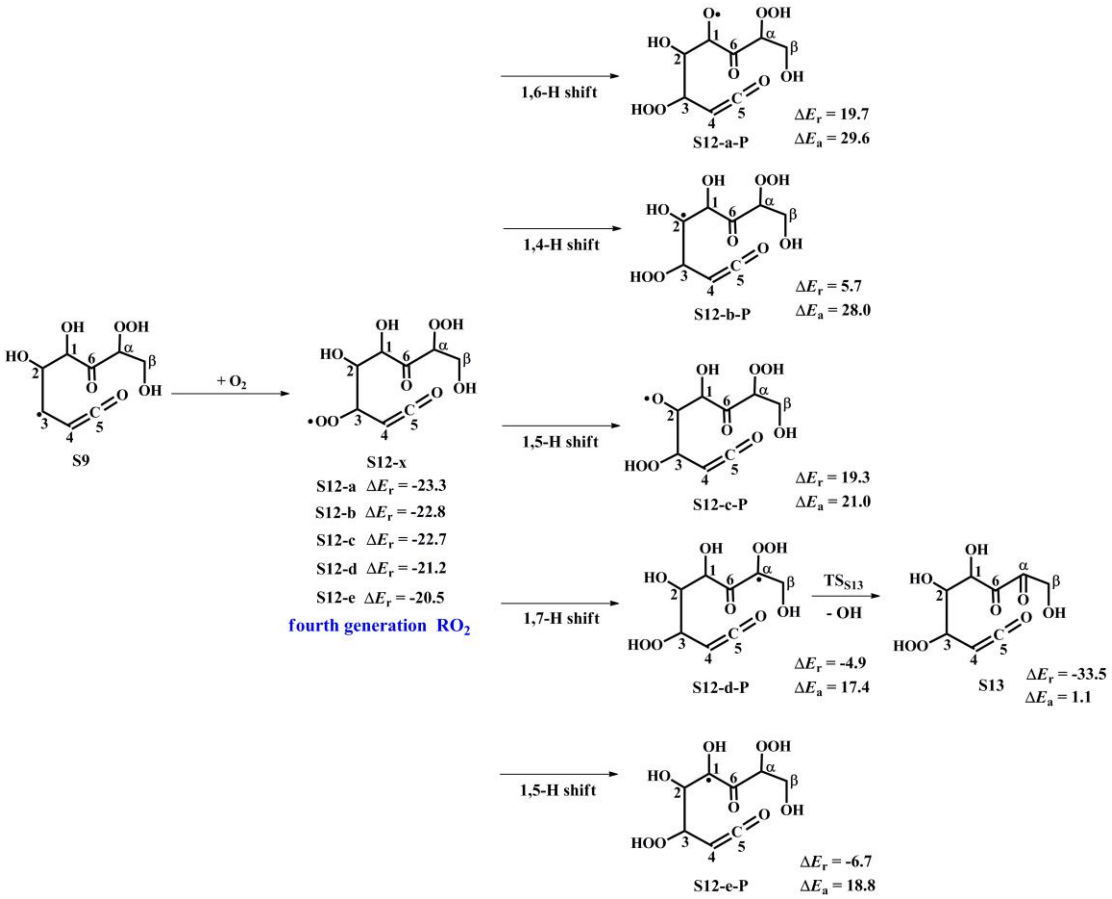

Figure S9. PES for the intramolecular hydrogen transfer reactions of S12-x at the M06-2X/6-311++G(3df,3pd)//M06-2X/6-31+g(d,p) level

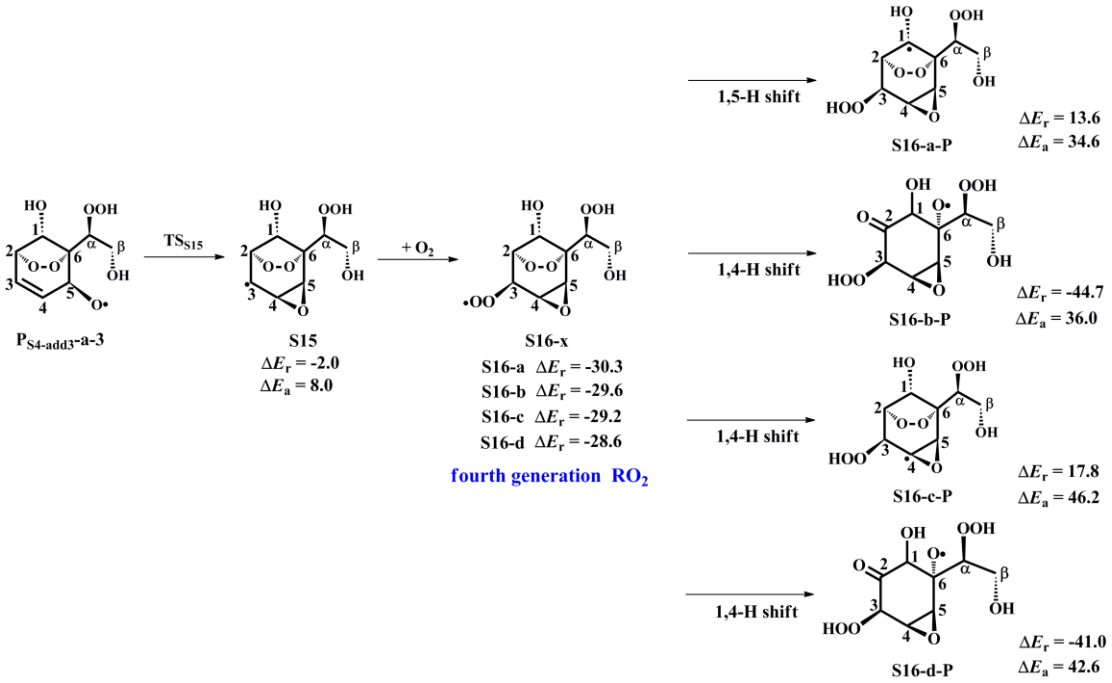

Figure S10. PES for the intramolecular hydrogen transfer reactions of S16-x at the M06-2X/6-311++G(3df,3pd)//M06-2X/6-31+g(d,p) level

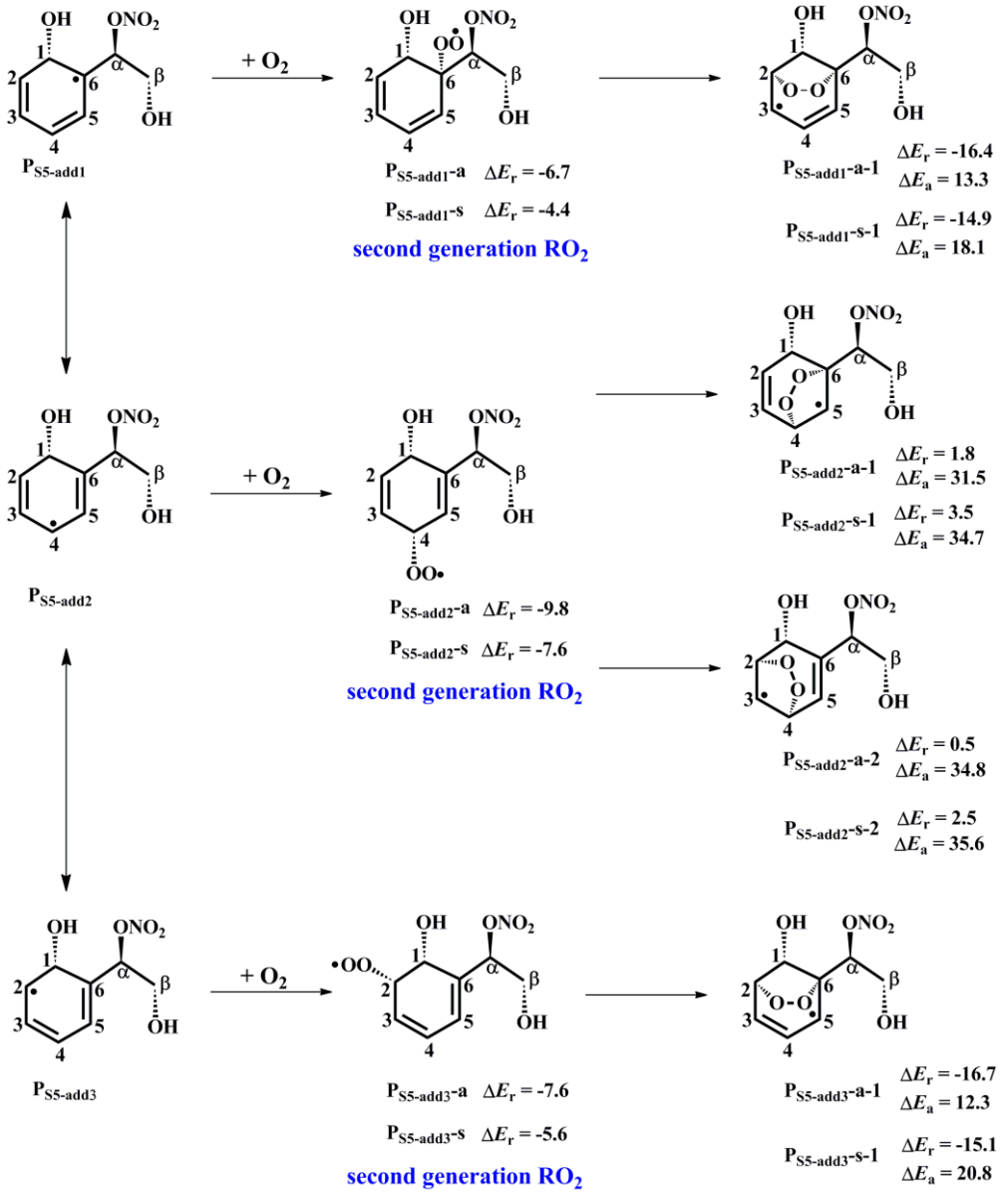

Figure S11. PES for the addition reactions $P_{S5\text{-}add1}$ + O_2 and subsequent intramolecular cyclization reactions at the M06-2X/6-311++G(3df,3pd)//M06-2X/6-31+g(d,p) level (the symbols s and a represent *syn*- and *anti*-O_2-addition)

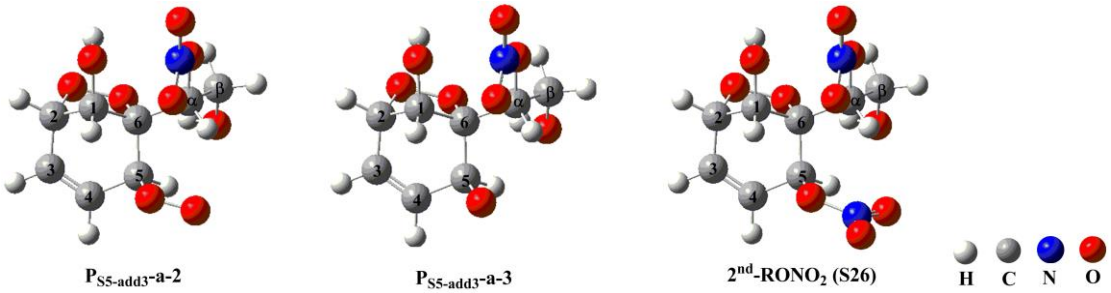

Figure S12. The lowest energy conformers of third generation peroxy radical $P_{S5\text{-}add3}$-a-2, peroxide bicyclic alkoxy radical $P_{S5\text{-}add3}$-a-3 and the second generation product bicyclic organic nitrate 2^{nd}-$RONO_2$(S26) at the M06-2X/6-31+g(d,p) level

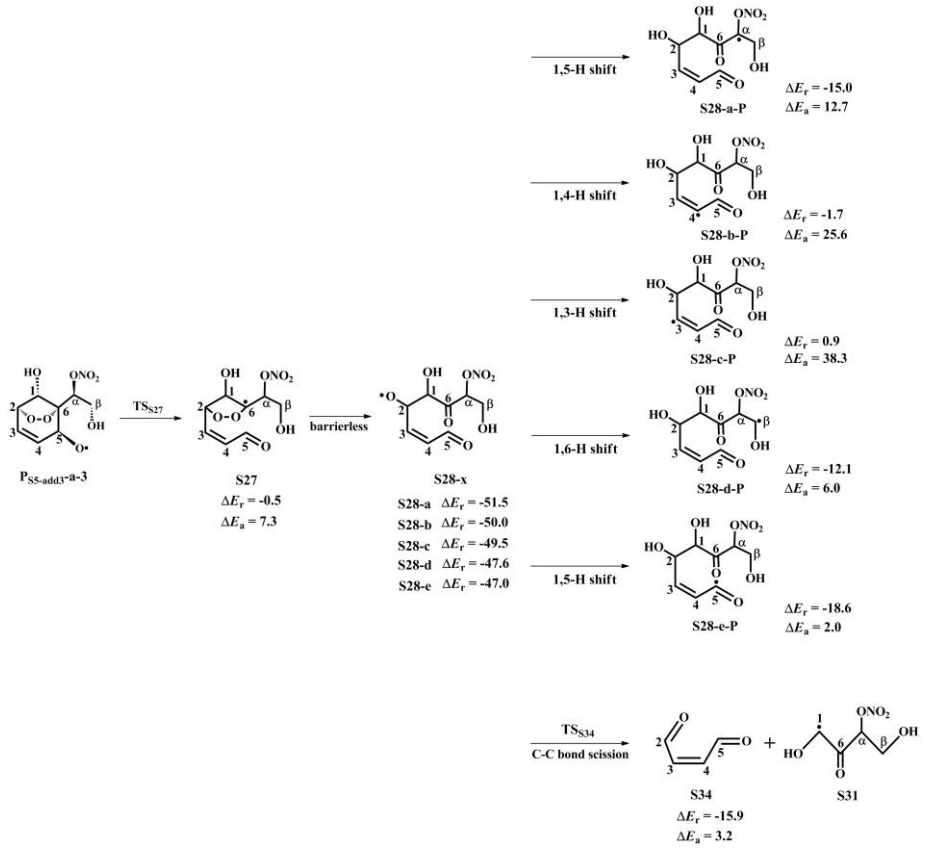

Figure S13. PES for the intramolecular hydrogen transfer reactions of S28-x at the M06-2X/6-311++G(3df,3pd)//M06-2X/6-31+g(d,p) level

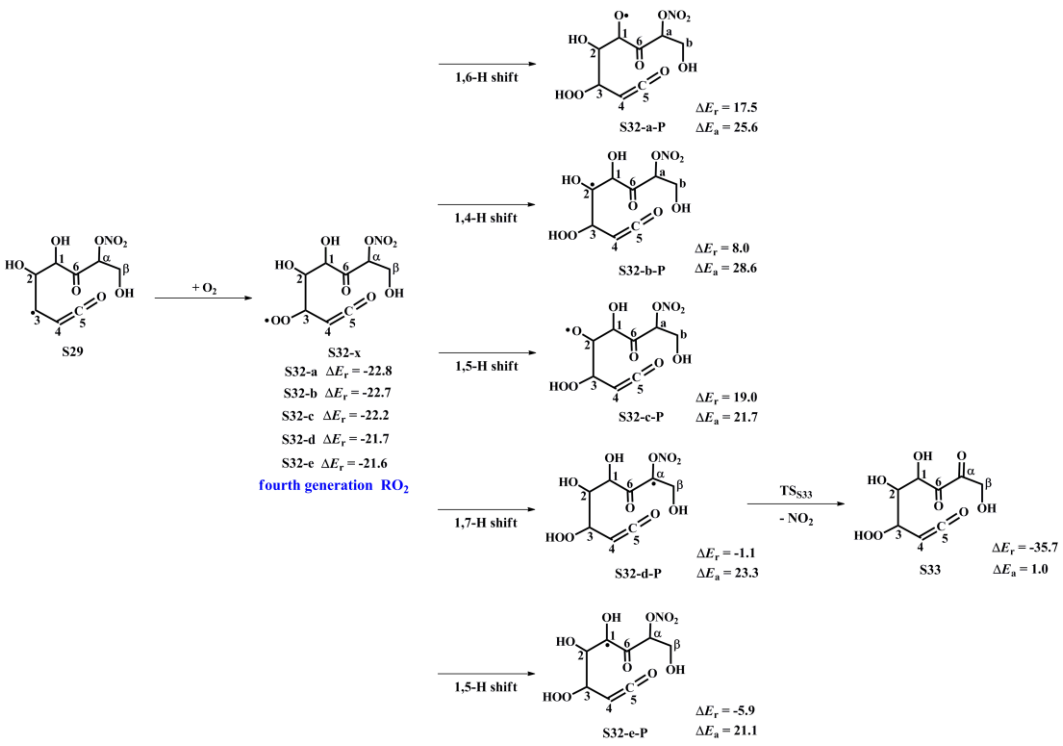

Figure S14. PES for the intramolecular hydrogen transfer reactions of S32-x at the M06-2X/6-311++G(3df,3pd)//M06-2X/6-31+g(d,p) level

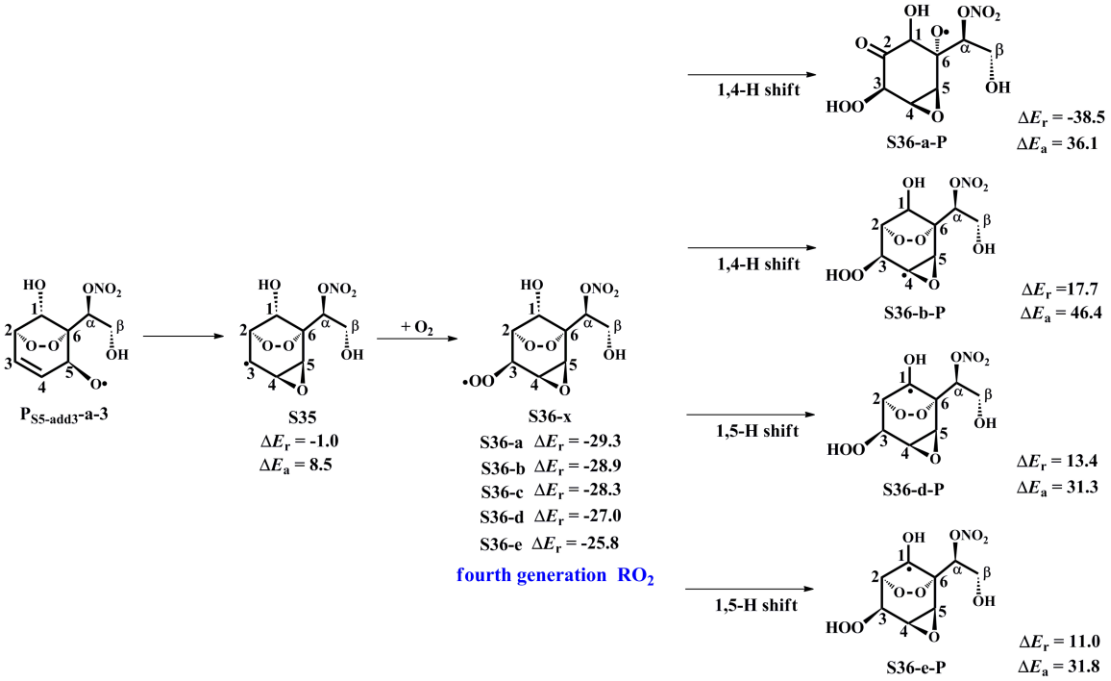

Figure S15. PES for the intramolecular hydrogen transfer reactions of S36-x at the M06-2X/6-311++G(3df,3pd)//M06-2X/6-31+g(d,p) level

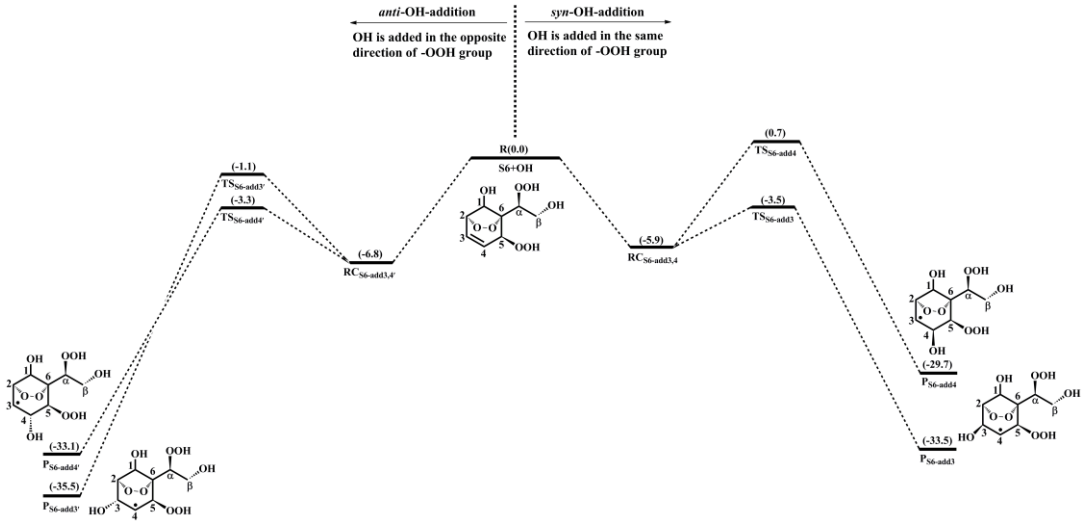

Figure S16. PES for the OH-addition reactions involved in the OH-initiated oxidation of 2nd-ROOH (S6) at the M06-2X/6-311++G(3df,3pd)//M06-2X/6-31+g(d,p) level

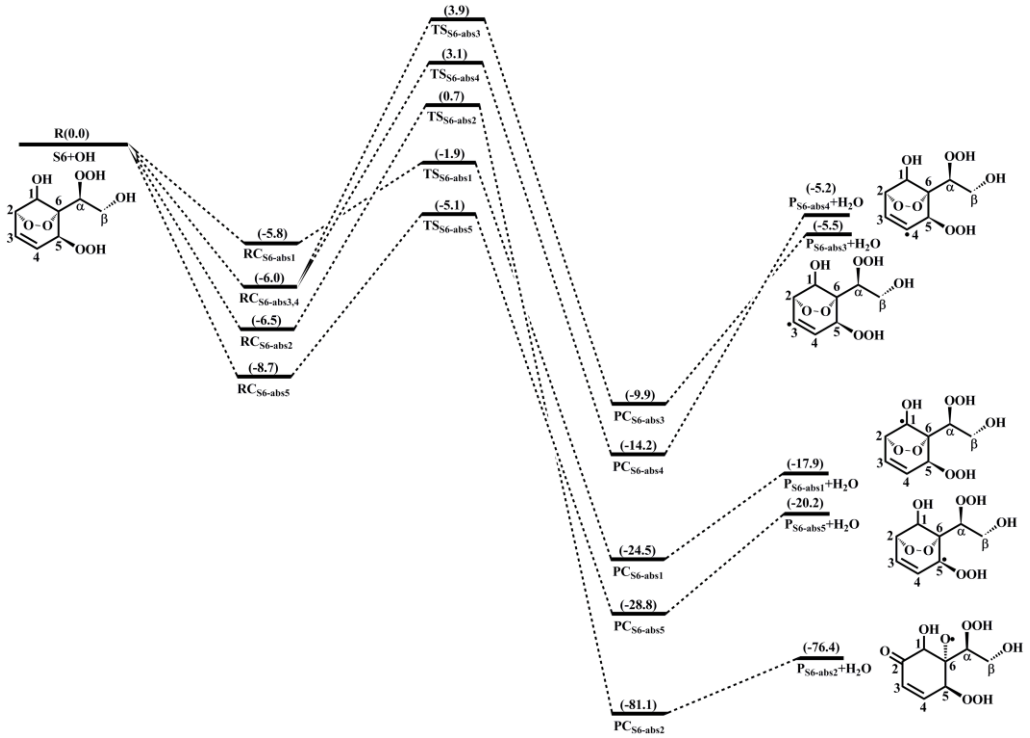

Figure S17. PES for the H-abstraction reactions involved in the OH-initiated oxidation of 2nd-ROOH (S6) at the M06-2X/6-311++G(3df,3pd)//M06-2X/6-31+g(d,p) level

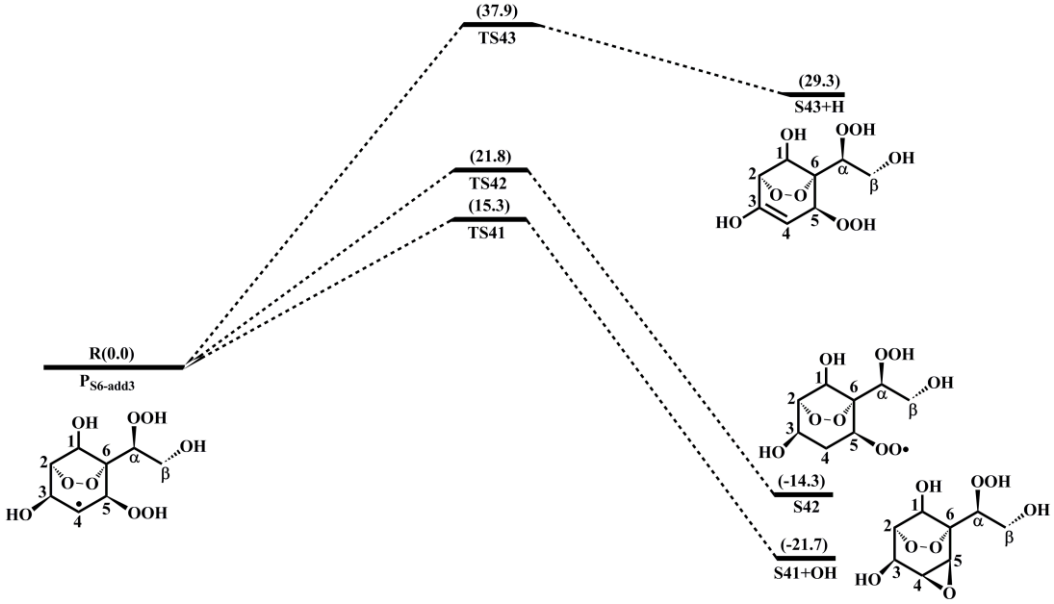

Figure S18. PES for the unimolecular decomposition of $P_{S6\text{-}add3}$ at the M06-2X/6-311++G(3df,3pd)//M06-2X/6-31+g(d,p) level

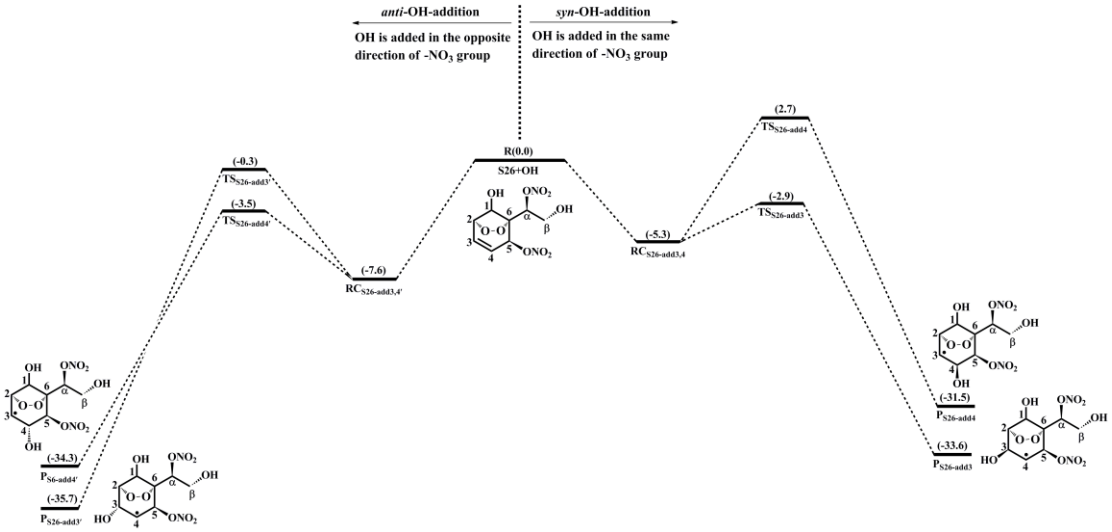

Figure S19. PES for the OH-addition reactions involved in the OH-initiated oxidation of 2^{nd}-$RONO_2$ (S26) at the M06-2X/6-311++G(3df,3pd)//M06-2X/6-31+g(d,p) level

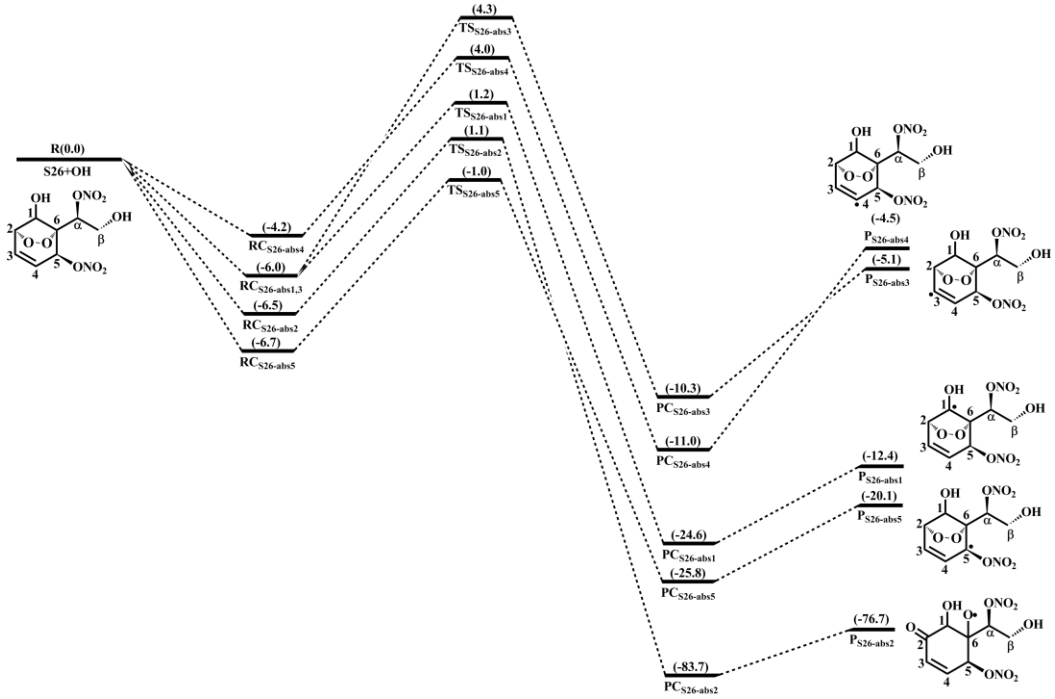

Figure S20. PES for the H-abstraction reactions involved in the OH-initiated oxidation of 2^{nd}-$RONO_2$ (S26) at the M06-2X/6-311++G(3df,3pd)//M06-2X/6-31+g(d,p) level

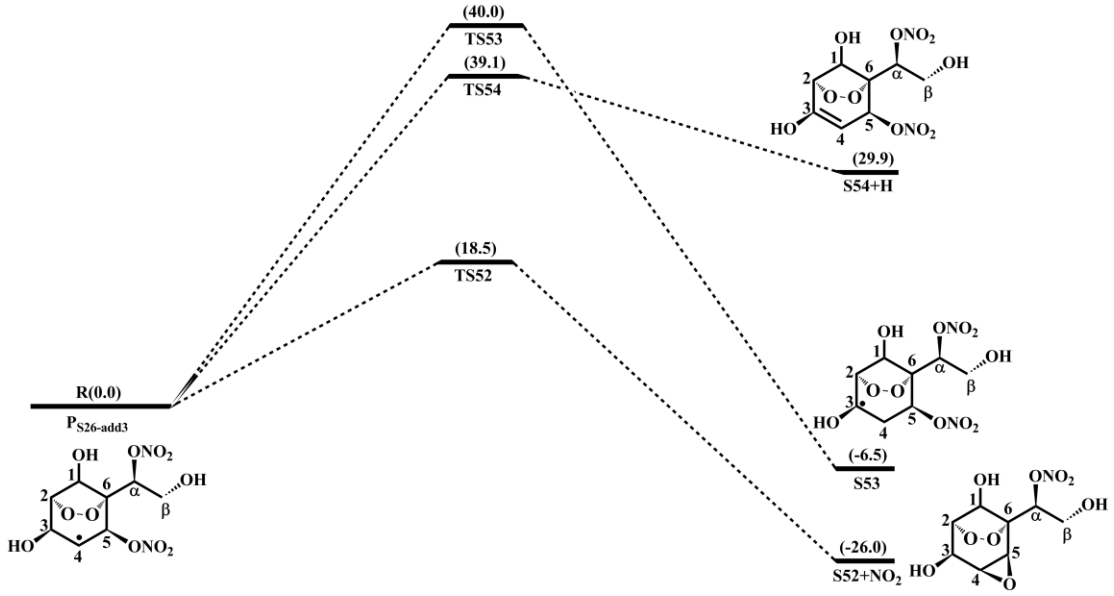

Figure S21. PES for the unimolecular decomposition of $P_{S26\text{-}add3}$ at the M06-2X/6-311++G(3df,3pd)//M06-2X/6-31+g(d,p) level

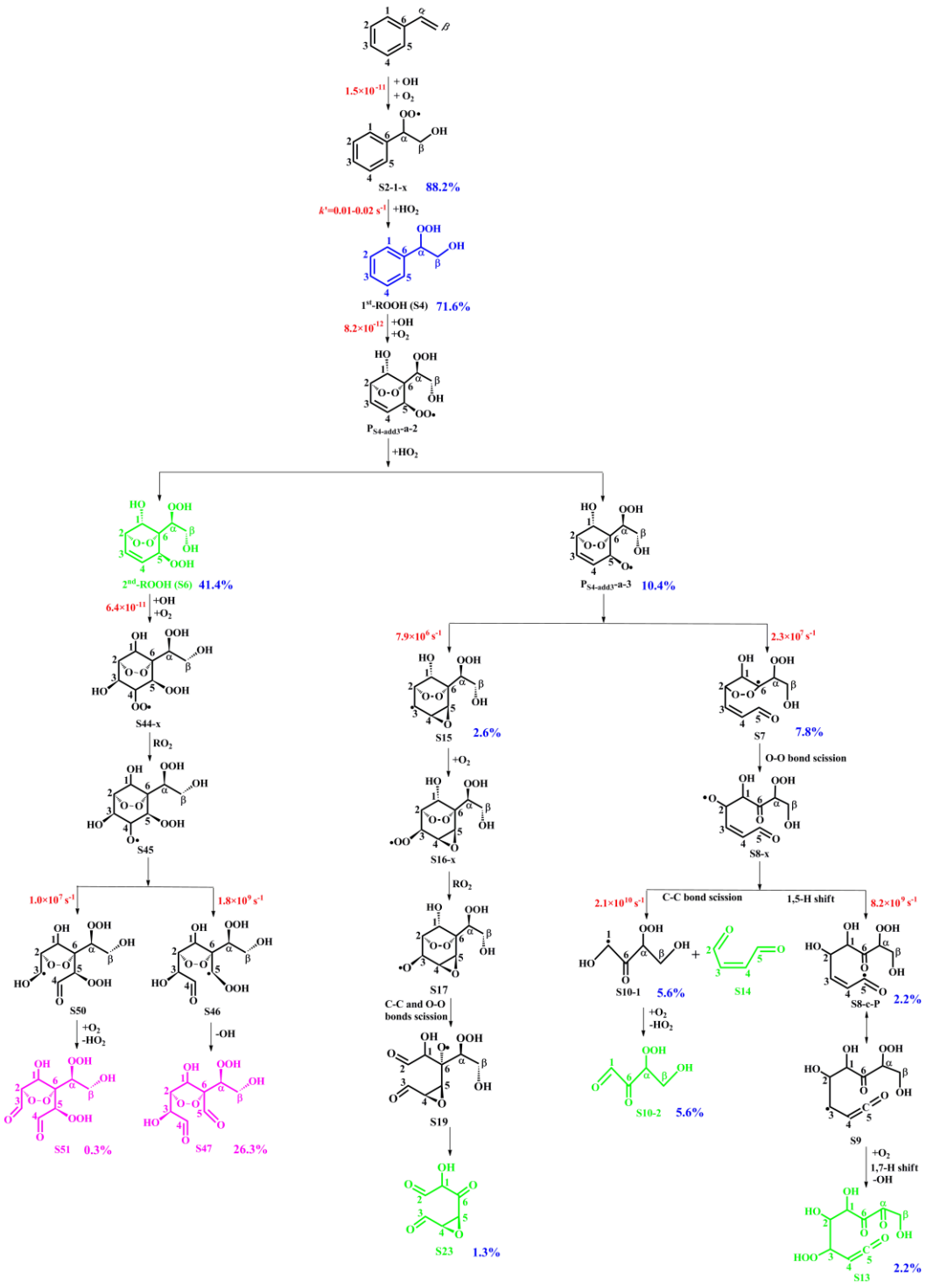

Figure S22. Overall reaction mechanism of the multi-generation OH oxidation of styrene in the low-NO_x conditions. The blue, green, and pink molecular structures represent the first, second and third generation closed-shell products, respectively. The rate coefficients are displayed in red. The calculated fractional yields of the closed-shell products are represented in blue. The reaction of peroxyl radical with HO_2 radicals is assumed to yield ROOH with a 80% branching ratio and RO radicals with a 20% branching ratio, based on the reaction of OH-substituted peroxy species with HO_2 radicals.

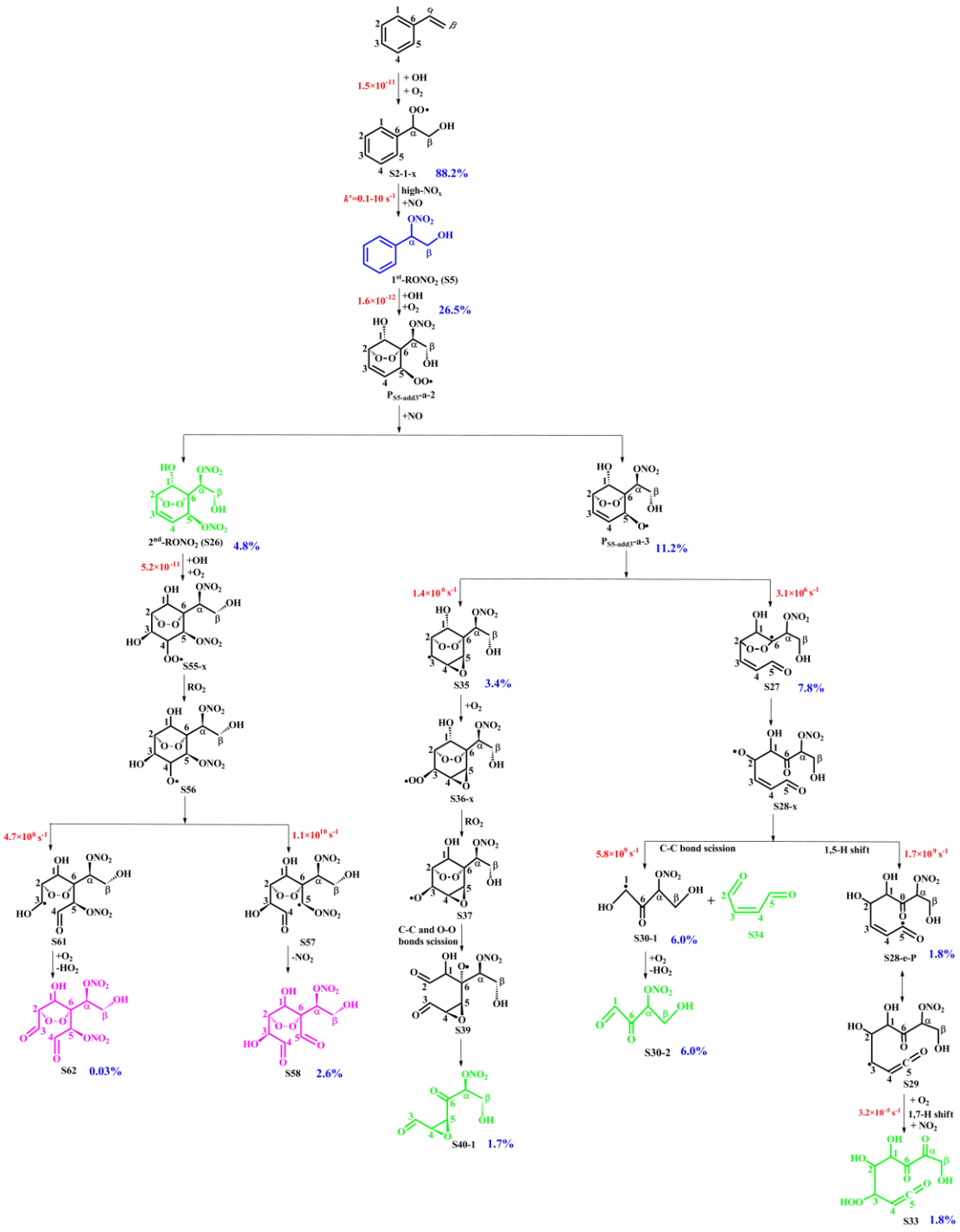

Figure S23. Overall reaction mechanism of the multi-generation OH oxidation of styrene in the high-NO_x conditions. The blue, green, and pink molecular structures represent the first, second and third generation closed-shell products, respectively. The rate coefficients are displayed in red. The calculated fractional yields of the closed-shell products are represented in blue. The reaction of peroxyl radical with NO is assumed to yield $RONO_2$ with a 30% branching ratio and RO radicals with a 70% branching ratio, based on the reaction of peroxy species containing 10 carbon atoms with NO.